The JSME International Conference on

Motion and Power Transmissions

MPT2001-Fukuoka

Fukuoka JAPAN, November 15-17, 2001

OPERATIVE VARIATOR CHARACTERIZATION FOR CVT IMPROVEMENT

* Francesco SORGE	*Department of Mechanics and Aeronautics, University of Palermo, Viale delle Scienze, 90128 – Palermo, ITALY* E-mail: sorge@dima.unipa.it
Alberto BECCARI	*Department of Mechanics and Aeronautics, University of Palermo, Viale delle Scienze, 90128 – Palermo, ITALY* E-mail: beccari@dima.unipa.it
Marco CAMMALLERI	*Department of Mechanics and Aeronautics, University of Palermo, Viale delle Scienze, 90128 – Palermo, ITALY* E-mail: cammalleri@dima.unipa.it

Keywords: Power Transmission, CVT, Rubber V-Belts, Limit Performance, Split-Way.

ABSTRACT

The present analysis addresses rubber V-belt variators.

Experimental results on the elasto-reological properties of several belts are presented and the belt wedging into the pulley groove under static loading is analyzed.

The convenience of innovative tensioning strategies is considered, e. g. attaining limit tension and full slip simultaneously, and an approximate formulation for the mechanics of V-belts is proposed.

Possible split-way arrangements are analyzed, aiming at the optimization of the variator class.

INTRODUCTION

Relevant problems arise in the area of V-belt CVT's due to the variable tension request in dependence on the operative conditions (torque and speed ratio). Pre-forcing is usually realized by hydraulic thrust on the pulleys with remarkable power losses, especially at partial load [1].

Passive tensioning systems, e. g. spring based, could in part overcome this drawback. Moreover, it would be convenient to calibrate the axial thrust so as to attain maximum admissible tension and slip limit simultaneously in the whole operative range, for the best variator exploitation [2-4]. To this end, it is important to gain precise information on the physical properties of the belts and develop a simple and reliable formulation for the belt variator mechanics in place of more complex though well established theories [5-7].

The idea of using the variator into split-way drives has stimulated the researchers in the last decade. The present concepts can be applied to a double way drive for the optimization of the power class of the variator.

EXPERIMENTS

Retarded elasticity phenomena appear during the static loading of rubber belts. Experimental tests on a traction machine permit a rough evaluation of the belt constitutive parameters.

The Maxwell element (spring and dashpot in series) plus a shunt spring gives an approximate model for the response of a belt element. The constitutive relationship between the belt tension T and the longitudinal elongation ε becomes

$$T + \tau_T \dot{T} = S(\varepsilon + \tau_\varepsilon \dot{\varepsilon}) \qquad (1)$$

where dots indicate derivatives with respect to time, S is the equilibrium stiffness, τ_T and τ_ε are viscous retardation times, dependent on the temperature and the deformation rate. It is interesting that a large viscous resistance inside the internal chord may retard the longitudinal deformation and reduce the sliding speed on the pulley. The possible advantages are analyzed in another paper [8].

Figure 1 shows a scheme of the experimental tests. Several commercial V-belts were wound on two cast-iron pulleys and loaded by a traction machine. Other tests were carried out by overturning and winding the V-belts on nylon band pulleys for a flat belt simulation. The center distance was increased in all the tests at the constant speed of 2.5 mm/min. The friction coefficient was calculated separately by dynamometric tests.

As an example, Fig. 2 a shows the experimental load/displacement diagram for the wedged and overturned set-up. The hysteresis effect is due to the belt internal viscosity and to the pulley friction. V-belts give rise to much higher displacements than flat belts owing to the elastic wedging into the groove, equivalent to a compliance increase.

Relaxation tests were also carried out to calculate the retardation times of the system (see Fig. 2 b). The asymptotic equilibrium tension $T_\infty = S\varepsilon$ was measured after several minutes of relaxation.

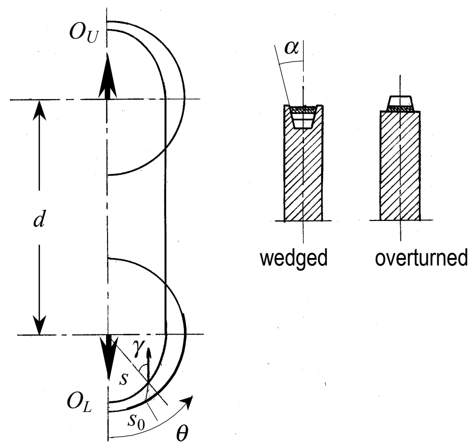

Fig. 1 Static Loading

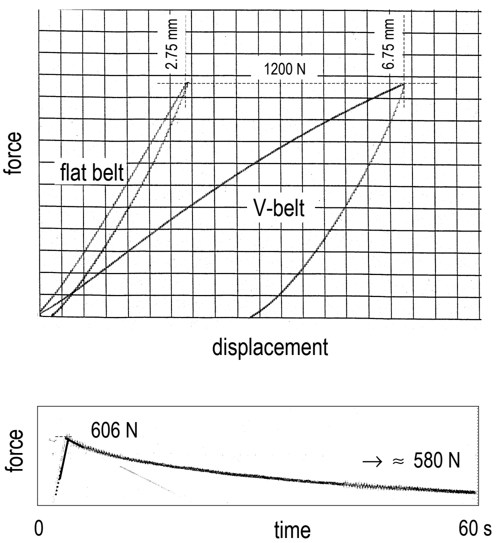

Fig. 2: (a) Hysteresis loop, (b) Relaxation

STATIC LOADING ANALYSIS

Theory

The present theory applies to the main sliding arc on the pulley. The short boundary arcs will be ignored and replaced by penetration discontinuities, as usual in V-belt mechanics [5-7].

The equilibrium and penetration equations of a V-belt element were derived in a previous paper [6]. Here, their abridged form is reported, neglecting smaller terms,

$$T' = T\tan\beta \qquad \text{(equilibrium)} \qquad (2)$$

$$\frac{T}{S} = \frac{kx}{1 - \dfrac{\tan\beta}{\cos^2\alpha\,\tan\gamma}} \qquad \text{(penetration)} \qquad (3)$$

where primes indicate derivatives with respect to the angular coordinate θ, $x = -\Delta r / r_0$ is the dimensionless penetration, the subscript $\ldots_0$ refers to zero load, α is the groove half-angle and k is a the radial stiffness parameter of the belt [6]. Moreover, γ (= sliding angle: see Fig. 1) and β (= arctan $\{ f\sin\gamma / [\, f\cos\gamma + \sin\alpha \sqrt{1+\tan^2\alpha\cos^2\gamma}\ ]\}$) are the angles formed with the radius in the plane of rotation, by the resultant friction force and the total wall force respectively.

V-belts with large width-to-thickness ratios deflect radially in the transverse planes and the theory of elasticity indicates a reduction of the local belt elongation: $\varepsilon(z) \cong \varepsilon_w - u(z)/r$, where z is the axial co-ordinate, ε_w the wall elongation, r the radius and u the centreward displacement.

For cogged V-belts, the cogs can be considered as transverse beams connected to each other by the chord layer. Each cog is subject to a distributed load due to $\varepsilon(z)$, yielding the deflection equation $\partial^4 U / \partial Z^4 + 4\mu^4 U = 4\mu^4 \varepsilon_w$, where $Z=2z/b$, $U = u/r$ and μ is a compliance parameter, to be determined by experiments. Imposing the boundary conditions $U = \partial U / \partial Z = 0$ for $Z = \pm 1$, integrating and averaging across the section, one gets $\varepsilon = \varepsilon_w \left(\mathrm{ch}^2\mu\sin^2\mu + \mathrm{sh}^2\mu\cos^2\mu\right) / [\mu(\mathrm{ch}\mu\,\mathrm{sh}\mu + \cos\mu\sin\mu)] = \varepsilon_w / B$, where B is constant in practice along the belt [9].

The belt will be here considered as one-dimensional and the symbol $\varepsilon = B\varepsilon_w$ will indicate the mean longitudinal elongation across the section.

When loading a V-belt as in Fig. 1, the two belt elements on the plane of symmetry (O_U and O_L) penetrate radially into the groove, the others penetrate and slide towards the free spans and the ends of the wrapped arc come out from the contact zone.

Let us indicate with s the length of a belt arc starting from the central plane and s_0 the zero load length (Fig. 1). Minding that all quantities are measured at the pulley walls and neglecting smaller terms, we write

$$s - s_0 = r_0\int_0^{\theta}(1-x)\,d\theta - r_0\theta_0 = r_0\int_0^{\theta_0}\varepsilon_w\,d\theta = r_0\int_0^{\theta_0}B\varepsilon\,d\theta \qquad \text{(4 a, b)}$$

$$\text{i. e.} \qquad \theta - \theta_0 = \int_0^{\theta_0}(B\varepsilon + x)\,d\theta$$

Consider a perfectly elastic belt ($\tau_T = \tau_\varepsilon = 0$, $\varepsilon = T/S$), impose the initial condition $\varepsilon = 0$ and assume a separable variable distribution, $\varepsilon(t,\theta) = \varepsilon_{fs}(t)\ Y(\theta)$, where the subscript $\ldots_{fs}$ refers to the free span and $Y(\pi/2) = 1$. The belt equilibrium (2) involves the independence of β (and γ) on the time t, which means that the belt elements penetrate along logarithmic spirals and the ratio $\varepsilon / x = w$ is independent of t due to Eq. (3), i. e. $x = \varepsilon_{fs}(t)\ X(\theta)$, where $X(\theta) = Y(\theta) / w(\theta)$.

The center distance increase while loading is given by

$$d - d_0 = d_0\varepsilon_{fs}(t) + 2r_0\int_0^{\pi/2}\varepsilon(t,\theta)[B + 1/w(\theta)]\,d\theta \qquad (5)$$

and in the hypothesis of a constant deformation rate v, we obtain $\varepsilon_{fs}(t) = vt/b$, where $b = d_0 + 2r_0\int_0^{\pi/2}Y(\theta)[B + 1/w(\theta)]d\theta$.

Differentiating Eq. (4 b) with respect to time, observing that $r\,d\theta = r\tan\gamma\,dx$, whence $\dot{x}\tan\gamma = \int_0^{\theta_0}(B\dot{\varepsilon} + \dot{x})d\theta$, eliminating the time dependent factors and differentiating with respect to θ_0, we get

$$d(X\tan\gamma)/d\theta_0 = (X\tan\gamma)' = BY + X \qquad (6)$$

Replacing x with X and T with YS into Eqs. (2) and (3), we have thus three equations in total in the space domain, Eqs. (2), (3) and (6), in the three unknowns X, Y and γ. Uniqueness considerations permit to accept the following results as the correct solution of the problem and justify the separable variable assumption.

It is easy to verify that the present separable variable solution applies to viscoelastic belts as well if $\tau_T = \tau_\varepsilon$, which is a realistic condition, since creep and relaxation times of polymers are not very different in most cases.

Solutions

Solve Eq. (3) for $\tan\gamma$, choosing $\tan\gamma > 0$ (Fig. 1). Then

$$\tan\gamma = \frac{C\sqrt{(k_1 - w)(w - k_2)}}{\cos^2\alpha\,(w - k)} \qquad (7)$$

where $C = \sqrt{\cos(\alpha+\varphi)\cos(\alpha-\varphi)}/\cos\varphi$, $k_1 = k\tan(\alpha+\varphi)/\tan\alpha$, $k_2 = k\tan(\alpha-\varphi)/\tan\alpha$, $\varphi = \arctan f$.

Eliminate γ through Eqs. (2) and (3):

$$Y' = C\sqrt{(k_1X - Y)(Y - k_2X)} \tag{8}$$

Since $(\tan\gamma)' = w'\, d(\tan\gamma)/dw$, $X' = w'\, dX/dw$ and $w' = Y'/(X + w\, dX/dw)$, Equations (6), (7) and (8) lead to a differential equation for the variable $X(w)$:

$$\begin{aligned}\frac{1}{X}\frac{dX}{dw} = \Big\{&\cos^2\alpha(1+Bw)(w-k)^2 - C^2\big[(k_m-w)(w-k) - \\ &-(k_1-w)(w-k_2)\big]\Big\}/ \\ /\, \Big\{&(w-k)\big[C^2(k_1-w)(w-k_2) - w(1+Bw)(w-k)\cos^2\alpha\big]\Big\}\end{aligned} \tag{9}$$

where $k_m = (k_1 + k_2)/2$.

Indicating with c_0 a constant of integration, the solution is

$$X = c_0\,(w-k)\,(w-w_1)^{a_1}\,(w-w_2)^{a_2}\,(w-w_3)^{a_3} \tag{10}$$

where the w_i are poles of Eq. (9), i. e. roots of the cubic equation $Bw^3 + \left(2 - Bk - f^2\tan^2\alpha\right)w^2 - \left(3 + 2f^2\right)kw + k^2\left(1 - f^2/\tan^2\alpha\right)$ = 0, (this same equation gives the asymptotic directions of the trajectory portrait [6]). The exponents can be calculated by $a_i = N(w_i)/\left[dD(w)/dw\right]_{w=w_i}$, where N and D are the numerator and the denominator of the right-hand side of Eq. (9).

One of the three roots is real and is always included between k and k_1; the other two may become complex when $k_2 < -1$ (large k and f, small α), though this is not frequent for common V-belts. In this eventuality, the partial fraction expansion of Eq. (9) leads to more complex solutions, which are here omitted for brevity.

Putting $dX/dw = (Y'/w' - X)/w$, Eqs. (8) and (9) give rise to a differential equation for the inverse function $\theta(w)$:

$$\begin{aligned}\frac{d\theta}{dw} = &\frac{C}{(w-k)\sqrt{(k_1-w)(w-k_2)}}\big[(2w-k)(k_1-w)(w-k_2) - \\ &-w(k_m-w)(w-k)\big]\ / \\ &/\,\big[C^2(k_1-w)(w-k_2) - w(1+Bw)(w-k)\cos^2\alpha\big] = \\ = &\frac{C}{\sqrt{(k_1-w)(w-k_2)}}\left[\frac{k}{C^2(w-k)} + \sum_{1\div 3}\left(\frac{b_i}{w-w_i}\right)\right]\end{aligned} \tag{11}$$

where the w_i have the same meaning as above and the b_i can be obtained similarly to the a_i.

The solution can be derived in closed form as sum I of the integrals I_i of the partial fractions. Putting $u = w - w_i$, $U = (k_1 - w)(w - k_2)$, $U_i = (k_1 - w_i)(w_i - k_2)$, we have

$$\int\frac{b_i\,dw}{u\sqrt{U}} \begin{cases} = \dfrac{-b_i}{\sqrt{U_i}}\log\left[\dfrac{\sqrt{UU_i} + U_i + u(k_m - w_i)}{0.5u}\right] & \text{if } U_i > 0 \\[2ex] = \dfrac{b_i}{\sqrt{-U_i}}\arcsin\left[\dfrac{u(k_m - w_i) + U_i}{0.5u(k_1 - k_2)}\right] & \text{if } U_i < 0 \end{cases}$$

and then

$$\theta = C\left[I(w) - I(k_1)\right] \tag{12}$$

as $w = k_1$ for $\theta = 0$ by Eq. (3), because γ vanishes in the plane of symmetry. The case of a pair of complex conjugate roots is more cumbersome and is not reported here for brevity.

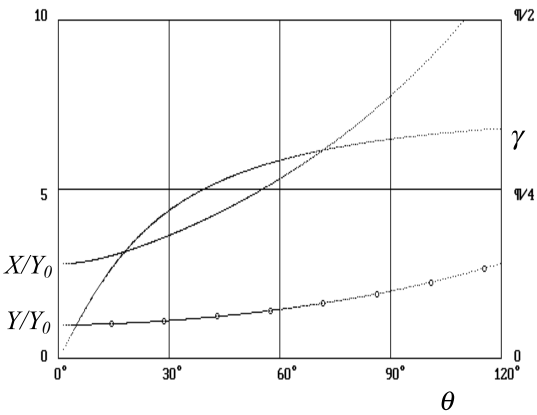

Fig. 3 Force and penetration diagrams for static loading ($k = 0.15$, $f = 0.3$, $\alpha = 14°$, $B = 2.5$)

Equations (10) and (12) provide a parametric representation of $X(\theta)$ and $Y(\theta) = w(\theta)\,X(\theta)$, where c_0 must be so chosen that $Y(\pi/2) = 1$. Then, the slope $2d\,T_{fs}/d\,(d - d_0) = 2S/b$ of the force/displacement diagram can be calculated in dependence of k, by integrating the function $BY(\theta) + X(\theta)$.

The flat belt arrangement implies $B = 1$, $X = 0$, $Y(\theta) = \exp f(\theta - \pi/2)$ and gives $b = d_0 + 2r\left[1 - \exp(-f\pi/2)\right]/f$. Thus, comparing V- and flat belt slopes and adjusting the radial stiffness k by tentative with the aim at the best fit with the experimental plots, the stiffness parameter k may be estimated. Figure 3 shows the diagrams $\gamma(\theta)$, $X(\theta)$ and $Y(\theta)$ for a typical case.

CVT ANALYSIS

V-Belt Mechanics

The equilibrium and penetration equations, Eqs. (2) and (3), must be rewritten putting $\varepsilon = (T - q\,v^2)/S$ in place of T/S, where $q\,v^2$ is the belt momentum flux and ε has now the meaning of "dynamic" elongation. A proper kinematic condition must replace the static deformation equation Eq. (6), accounting for the triangle of velocities and the mass conservation requirement [6]

$$x'\tan\gamma = x - x_o + B\varepsilon - B\varepsilon_o \tag{13}$$

By elimination of γ like in the previous section, a differential system for ε and x can be obtained

$$\varepsilon' = \pm C\sqrt{(k_1x - \varepsilon)(\varepsilon - k_2x)} \tag{14}$$

$$x' = \pm\cos^2\alpha\,\frac{(x - x_o + B\varepsilon - B\varepsilon_o)(\varepsilon - kx)}{C\sqrt{(k_1x - \varepsilon)(\varepsilon - k_2x)}} \tag{15}$$

where the double sign refers to the driven (+) and driver (–) pulley and the subscript $\ldots_o$ refers to the "orthogonal point" at the beginning of the main sliding arc, where the belt velocity and the friction force are orthogonal, $\gamma = 0$ and $\varepsilon_o/x_o = k_1$ [6].

Equations (14) and (15) are singular at the orthogonal point, but can be solved by Runge-Kutta routines. Eliminating the independent variable by division of Eqs. (14) by (15), a trajectory portrait can be sketched on the tension/penetration plane (Fig. 4). The orthogonal point O is a singularity for the trajectory equation, whence the driven and driver trajectories spring out with slopes $p_o = \pm\sqrt{(1.5 - f\tan\alpha)^2/B^2 + 2k(1 + f/\tan\alpha)/B} - (1.5 - f\tan\alpha)/B$

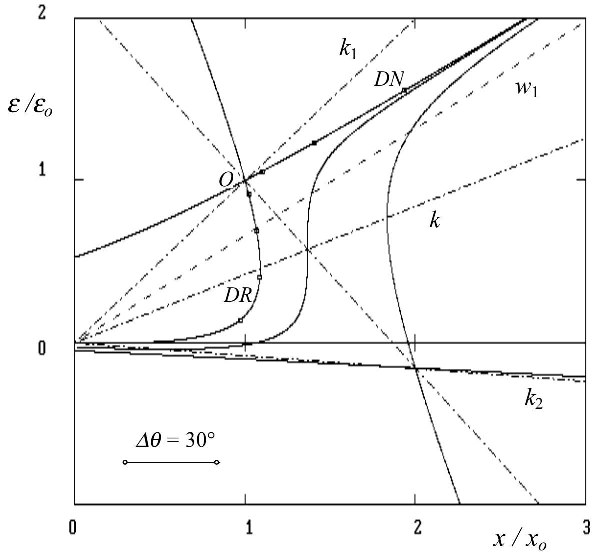

Fig. 4 Trajectory portrait (data of Fig. 3)

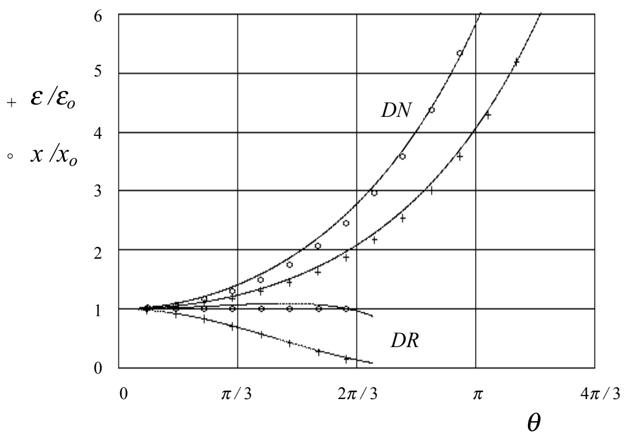

Fig. 5 Closed form solutions (°⁺) for V-belt drives (data of Fig. 3)

In practice, taking values from the present experimentation for f and k, the driver pulley trajectory denounces rather small penetration changes along the main sliding arc, while the driven pulley trajectory is similar to a straight-line with a certain slope p through the orthogonal point (Fig. 4). Moreover, the numerical solutions indicate a nearly linear increase of γ and β along the sliding arc of the driver pulleys.

This suggests to put $\varepsilon' = \varepsilon \tan(\beta_o' \theta)$ and $x \cong x_o$ for the driver pulley, replace $x - x_o \cong (\varepsilon - \varepsilon_o) / p$ into Eq. (14) for the driven pulley and ignore Eq. (15). By the previous definition of β, we derive $\beta_o' = \gamma_o' f / (f + \tan\alpha)$, where γ_o' can be obtained differentiating twice Eq. (13) at the orthogonal point and minding that $\varepsilon_o'' / x_o'' = p_o$ due to l'Hôpital rule: $\gamma_o' = 0.5\ (1 + B\, p_o)$. Therefore, we get by integration

$$\frac{\varepsilon}{\varepsilon_o} = \left[\cos(\beta_o' \theta)\right]^{-1/\beta_o'} \qquad (DR) \qquad (16)$$

$$\frac{\varepsilon}{\varepsilon_o} = 1 + \frac{p}{2k_1}\left(\frac{k_1 - k_2}{p - k_2}\right)\left[\cosh(\Omega\theta) - 1\right] \qquad (DN) \qquad (17)$$

where $\Omega = \sqrt{(k_1 - p)(p - k_2)}\, C/p$ and we remark that $k \propto r_0^{\,2}$ and thus is different for the DN and DR pulleys and changes with the speed ratio. The slope p may be chosen as a suitable mean of the slope at the orthogonal point, p_{oDN}, and the asymptotic slope $p_\infty = w_1$ (see previous section). A very good fit can be obtained putting $p = 0.6\, p_{oDN} + 0.4\, p_\infty$, as shown in Fig. 5, where the Runge-Kutta plots of ε and x are traced by a continuous line and compared with the solutions (16) and (17).

The penetration function $x\,(\theta)$ permits the calculation of the axial thrust F_z, by integration of the unit angle axial force $F_z' = kxS / 2\tan\alpha$.

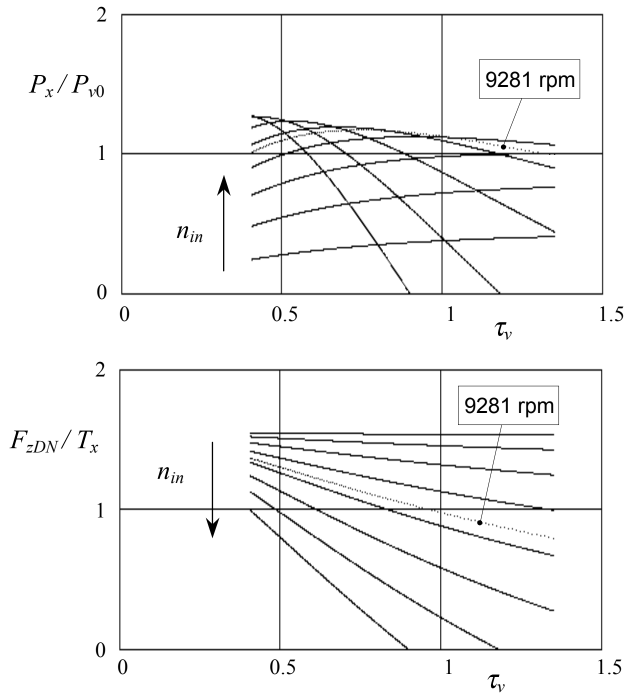

Fig 6: (a) Limit power, (b) Driven pulley axial thrust

- Variator characteristics: center distance = 255 mm, mean radii = 39 mm, wedge angle = 14°
- Belt: cogged type, unit length mass = 0.124 kg/m, transverse width = 15 mm, friction coefficient = 0.3, admissible tension = 500 N
- n_{in} = 2000, 4000, …, 16000 rpm

Limit Performance

Suppose to load a variable speed drive close to the full slip limit and control the axial thrust so as to attain the highest admissible tension T_x on the tight span. Since self-locking usually prevents full slip on the driver pulley, this limit condition can be reached in practice only on the driven one.

Then, indicating with Θ the arc of contact and using the previous model, we obtain the limit relationships for the transmissible power and the axial thrust:

$$P_x = T_x \omega_{DR} r_{DR}\left(1 - \frac{q\,\omega_{DR}^{\,2} r_{DR}^{\,2}}{T_x}\right)\left[1 - \frac{1}{1 + \dfrac{p}{2k_1}\left(\dfrac{k_1 - k_2}{p - k_2}\right)(\cosh\Omega\Theta - 1)}\right]_{DN} \qquad (18)$$

$$F_{zDR} = \frac{T_x - q\omega_{DR}{}^2 r_{DR}{}^2}{2\tan(\alpha+\varphi)}\,\Theta_{DR} \tag{19}$$

$$F_{zDN} = \frac{T_x - q\omega_{DR}{}^2 r_{DR}{}^2}{2\tan(\alpha+\varphi)} \left[\frac{2\Theta + \left(\frac{k_1 - k_2}{p - k_2}\right)\left(\frac{\sinh \Omega\Theta}{\Omega} - \Theta\right)}{2 + \frac{p}{k_1}\left(\frac{k_1 - k_2}{p - k_2}\right)\left(\cosh \Omega\Theta - 1\right)} \right]_{DN} \tag{20}$$

For example, the diagrams of Fig. (6 a, b) were drawn in dependence on the speed ratio τ_v for a commercial variator, for several input speeds. The particular driving speed 9281 rpm produces equal power at the ends of the range, and this level (P_{v0}) is used for scaling the power diagram, due to the opportunity of a conventional reference performance. The quasi-linear dependence of the axial thrust on the speed ratio indicates the feasibility of the limit operation by means if a simple loading spring on the driven pulley without any external control [4].

More accurate but complex relationships for the axial thrust could also be used [10].

SPLIT-WAY SCHEME

As well known, the speed range of a CVT can be amplified by inserting the variator into a double- or multi-way arrangement, connecting the branches by one or more epicyclic trains (see [2, 3], also for a survey on the literature). This practice may yield infinite or even negative "aperture" (ratio of the maximum and minimum speed ratio) but must be paid by an increase of the power demand to the variator, i. e. of its "class" (ratio of the multi-way and single-way variator power).

Speed-Power Gain Balance

Define as "speed gain" of a complex CVT scheme the ratio between the logarithmic differentials of the speed ratios of the whole transmission and of the simple variator: $(d\tau/\tau)$ / ($d\tau_v/\tau_v$). Besides, define as "power gain" the ratio between the total power and the variator power. The principle of virtual displacements permits to demonstrate that the product of such two gains must be equal to unity in no friction conditions.

Whichever multi-way CVT is considered as in Fig. 7, suppose to take away the inside variator and leave the primary and secondary torque applied at the shaft stumps as external reaction couples. Assuming no-friction working, the virtual displacement principle requires the vanishing of the total work done by the input, output, primary and secondary torque for any virtual rotation of all shafts from an equilibrium configuration:

$$\begin{aligned} &M_{in}(\vartheta_{in} + \delta\vartheta_{in}) - M_{out}(\vartheta_{out} + \delta\vartheta_{out}) = \\ &\quad = M_{DR}(\vartheta_{DR} + \delta\vartheta_{DR}) - M_{DN}(\vartheta_{DN} + \delta\vartheta_{DN}) \end{aligned} \tag{21}$$

where the $\vartheta_i = \omega_i \Delta t$ are real shaft rotations, such that $\vartheta_{out}/\vartheta_{in} = \tau$, $\vartheta_{DN}/\vartheta_{DR} = \tau_v$ and that the total work of the four couples M_i is zero, while the $\delta\vartheta_i$ are arbitrary virtual variations allowed by the system constraints.

Since $M_i\vartheta_i = P_i\Delta t$, $\tau + \delta\tau = (\vartheta_{out} + \delta\vartheta_{out}) / (\vartheta_{in} + \delta\vartheta_{in})$, i. e. $\delta\tau/\tau = \delta\vartheta_{out}/\vartheta_{out} - \delta\vartheta_{in}/\vartheta_{in}$ and $\tau_v + \delta\tau_v = (\vartheta_{DN} + \delta\vartheta_{DN}) / (\vartheta_{DR} + \delta\vartheta_{DR})$, i. e. $\delta\tau_v/\tau_v = \delta\vartheta_{DN}/\vartheta_{DN} - \delta\vartheta_{DR}/\vartheta_{DR}$, then

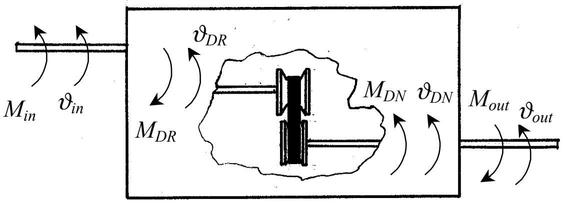

Fig. 7 Multi-way CVT

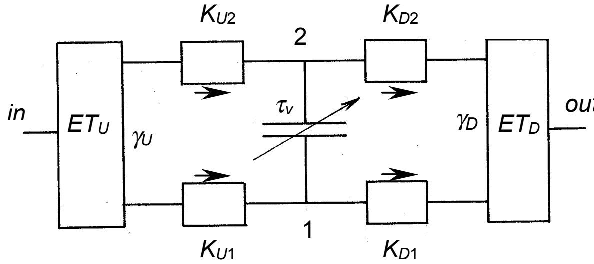

Fig. 8 Symmetric split way scheme

Equation (21) gives $P_{var.}\ \delta\tau_v/\tau_v = P_{tot.}\ \delta\tau/\tau$, which is exactly what we wanted to prove.

Two-Epicyclic Train Scheme

As an example, let us consider the symmetric double-way-two-epicyclic-train scheme of Fig. 8 and suppose ideal no-friction working. The boxes indicate gears, where the power fluxes and speed ratios must be considered according to the arrow directions in the figure, e. g. $\tau_v = \omega_2/\omega_1$, etc.

The analysis can be carried out in the usual way by equating to zero the total entering power and the sum of the external couples for each epicyclic gear.

$$\frac{\tau}{\tau_m} = \xi \left(\frac{1 + \sigma_D \tau_v/\tau_{vm}}{1 + \sigma_U \tau_v/\tau_{vm}} \right) \tag{22}$$

$$\frac{P_{var.}}{P_{tot.}} = \frac{1}{1 + \sigma_U \tau_v/\tau_{vm}} - \frac{1}{1 + \sigma_D \tau_v/\tau_{vm}} \tag{23}$$

Here, the subscripts $\ldots_m$, $\ldots_U$ and $\ldots_D$ refer to the minimum external speed ratio of the whole transmission and to the upstream and downstream epicyclic train. Moreover, we have put $\sigma_D = \tau_{vm}\gamma_D K_{D2}/K_{D1}$, $\sigma_U = \tau_{vm}\gamma_U K_{U1}/K_{U2}$, $\xi = K_{U1}K_{D1}(1+\gamma_U)/[\tau_m(1+\gamma_D)]$, where γ_U and γ_D are the torque ratios through the shafts 2 and 1, i. e. fixed functions of the basic speed ratios of the respective epicyclic trains, independently of τ.

Indicating with $A = \tau_M/\tau_m$ and $A_v = \tau_{vM}/\tau_{vm}$ the "apertures" of the whole drive and of the variator, where the subscript $\ldots_M$ refers to the maximum external speed ratio, we get $\sigma_U = [A - A_v + \xi\,(A_v - 1)] / [A_v\ (1 - A)]$ and $\sigma_D = [A\,A_v - 1 - A\,(A_v - 1) / \xi] / [A_v\ (1 - A)]$. Therefore, the behavior of a particular transmission is completely defined by a triad of numbers ξ, A and A_v , independently of the specific values of the fixed ratios K or γ, which may thus be chosen in view of the simplest arrangements. For example, putting $K = 1$ is equivalent to the elimination of a gear, putting $\gamma = 0$ or ∞ is equivalent to the elimination of an epicyclic train, which must be associated with an additional condition $K = 0$ or ∞ that eliminates a branch.

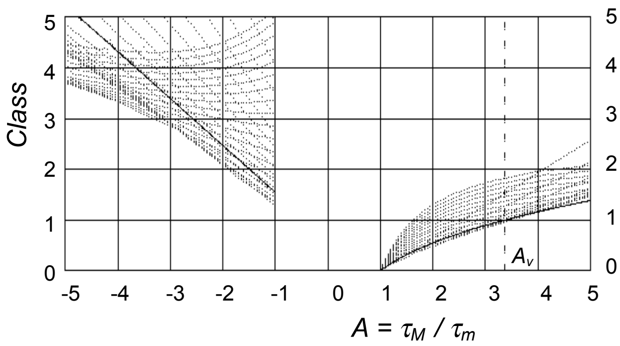

Fig. 9 Variator class map (data of Fig. 6), $A_1 = 0.5, 0.6, \ldots, 2$

Thick line: optimization for constant power variator (P_{v0})

Once chosen ξ, A and A_v , the ratio of the driving speed of the variator and the input speed is determined as a function of τ_v, $\omega_1/\omega_{in} = K_{U1}(1+\gamma_U)/(1+\sigma_U \tau_v/\tau_{vm})$, so that, assuming constant engine speed, the limit operative curves of the variator can be traced on the characteristic map of Fig. 6 a, b.

At full input power, it is vital that the power request (23) should be compatible with the power capacity of the variator, which condition identifies the variator class for given engine, once the drive scheme has been chosen.

Of course, this compatibility cannot be fulfilled in the whole speed range in case of infinite or negative aperture, if one minds for example that the neutral configuration implies the divergence of the power ratio (23), at least for ideal no-loss working. Some limiting device should be then present in the layout in addition to the common engine throttle, in order to cut the engine feed, for example in the range between the reverse and the symmetrical forward speed ($-1 < \tau / \tau_m < 1$).

This limiting device could be conceived in such a way to deliver the maximum admissible power to the variator throughout the mentioned partial range around the neutral. Otherwise, it could be planned for providing constant output torque in that range. Here, the last condition is imposed.

Furthermore, the variator should be optimized in the whole speed range by equating admissible and requested power in the most critical conditions. Comparing with the one-epicyclic train scheme, an important advantage of the two-epicyclic train choice is the possibility of imposing two critical conditions instead of one. Thus, a finer fit can be achieved, though at the cost of a greater complexity of the set-up.

Indicating with P_{v0} the reference variator power (e. g. the endpoint power for n_{in} = 9281 rpm in Fig. 6), define the variator class in a split-way scheme as the ratio between $P_{var.}/P_{tot.}$ (23) and P_x/P_{v0} (18) in the most critical condition (where $P_{var.} = P_x$). For geometrically similar variators and same belt speed, the class is proportional to the square of the size by Eq. (18).

Figure 9 shows the variator class in dependence on the total aperture A for A_v = 3.375 or 1/3.375 and for several values of the "partial" aperture $A_1 = \omega_{1M}/\omega_{1m} = (\xi - A) / [\, A_v\, (\xi - 1)]$, which is here chosen as the third free parameter in place of ξ. The minimum class can be obtained by enveloping the plots from below: this determines the quantities A_1 and ξ.

As can be seen, the class is nearly equal to A / A_v when A > 0, but grows to much higher numbers when A < 0. This is a consequence of the power flux recirculation through the variator (see previous subsection). Nevertheless, the present procedure guarantees the lowest obtainable class rises among all possible schemes like Fig. 8.

The use of two- or multi-mode transmissions, where the switch from one mode to another is done during synchronous running by suitable clutches, permits a substantial reduction of the variator class, but at the cost of more complex schemes.

CONCLUSION

Simple experimental tests permit the characterization of rubber V-belt variators as regards the tribological properties of the belt-pulley contact and the (visco-) elastic parameters concerning longitudinal elongation, radial bending and penetration of the belt. A suitable theory on the static loading of the belt-pulley system can be used for this type of analysis.

Accurate closed form approximations to V-belt mechanics apply very well to the limit performance of variators, i. e. at full slip and maximum admissible tension.

Such a limit behavior permits the best exploiting of the variator characteristics inside a split-way CVT, aiming at the lowest variator class for given driving engine.

ACKNOWLEDGMENT

The authors acknowledge the financial support of the Italian Ministry M.U.R.S.T.

REFERENCES

1. Bas Van Vuren, "Efficiency Improvement in CVT Systems", *Proceedings of SITEV 90, Technical Forum*, Torino, Italy, (1990).
2. Alberto Beccari and Francesco Sorge, "Improved Performances of CV Transmissions for Passenger Cars", *Proceedings of the 3rd ATA Intern. Conference Innovation and Reliability in Automotive Design and Testing*, Firenze, Italy, (1992).
3. Massimo Andolina and Alberto Beccari, "Continuous Variation Transmission in Automotive Application: Extension of the Working Range of Automotive Transmission to Start and Reverse Motion with Minimization of Variator Dimension", *Proceedings of the JSAE Intern. Conference CVT '96*, Yokohama, Japan, (1996).
4. Alberto Beccari and Marco Cammalleri, "Implicit Regulation for Automotive Variators", *Proceedings of Inst. of Mech. Engin.*, (to be published).
5. Göran Gerbert, "Force and Slip Behaviour in V-Belt Drives", *Acta Polytechnica Scandinavica*, *Mech. Eng. Series*, Helsinki, Finland, (1972).
6. Francesco Sorge, "A Qualitative-Quantitative Approach to V-Belt Mechanics", *ASME Journ. of Mech. Design*, Vol. **118**, (1996), 15-21.
7. Göran Gerbert, "Traction Belt Mechanics", Chalmers, Göteborg, Sweden, (1999).
8. Francesco Sorge and Marco Cammalleri, "Viscoelastic Response of Rubber Belts", *Proceedings of the 15th Congress AIMETA*, Taormina (ME), Italy, (2001).
9. Francesco Sorge, "Limit Performances of V-Belt Drives", *Proceedings of the Intern. Conference CVT '99*, Eindhoven, The Netherlands, (1999).
10. Francesco Sorge, "A Simple Model for the Axial Thrust in V-Belt Drives", *ASME Jour. of Mech. Design*, Vol. **118**, (1996), 589-592.